Published in final edited form as:
Nat Genet. 2017 May ; 49(5): 730–741. doi:10.1038/ng.3817.

A single-copy *Sleeping Beauty* transposon mutagenesis screen identifies new *PTEN*-cooperating tumor suppressor genes

Jorge de la Rosa[1,2,3,*], **Julia Weber**[4,5,*], **Mathias Josef Friedrich**[1], **Yilong Li**[1], **Lena Rad**[1], **Hannes Ponstingl**[1], **Qi Liang**[1], **Sandra Bernaldo de Quirós**[1], **Imran Noorani**[1], **Emmanouil Metzakopian**[1], **Alexander Strong**[1], **Meng Amy Li**[1], **Aurora Astudillo**[6], **María Teresa Fernández-García**[7], **María Soledad Fernández-García**[7], **Gary J. Hoffman**[1,8], **Rocío Fuente**[1], **George S. Vassiliou**[1], **Roland Rad**[1,4,5,‡], **Carlos López-Otín**[3,9,‡], **Allan Bradley**[1,‡], and **Juan Cadiñanos**[1,2,‡]

[1]The Wellcome Trust Sanger Institute, Wellcome Trust Genome Campus, Hinxton, Cambridgeshire, CB10 1SA, UK

[2]Instituto de Medicina Oncológica y Molecular de Asturias (IMOMA), 33193-Oviedo, Spain

[3]Departamento de Bioquímica y Biología Molecular, Facultad de Medicina, Instituto Universitario de Oncología (IUOPA), Universidad de Oviedo, 33006-Oviedo, Spain

[4]Department of Internal Medicine II, Klinikum rechts der Isar, Technische Universität München, Ismaninger Strasse 22, 81675 München, Germany

[5]German Cancer Consortium (DKTK), German Cancer Research Center (DKFZ), Heidelberg, Germany

[6]Servicio de Anatomía Patológica, Hospital Universitario Central de Asturias, 33011- Oviedo, Spain

[7]Unidad de Histopatología Molecular, Facultad de Medicina, IUOPA, Universidad de Oviedo, 33006-Oviedo, Spain

[8]School of Medicine, University of Western Australia, Crawley WA 6009, Australia

Correspondence should be addressed to: Juan Cadiñanos, Instituto de Medicina Oncológica y Molecular de Asturias (IMOMA), Avda. Richard Grandío s/n, 33193 Oviedo, Spain, jcb@imoma.es.
*Equal contribution
‡Equal contribution

Author Contributions

J.d.l.R., R.R., C.L.-O., A.B. and J.C. designed the study. J.d.l.R., J.W., R.R. and J.C. generated mouse alleles/cohorts and performed experiments. J.d.l.R., J.W., L.R., Q.L., M.A.L., G.S.V., R.R. and J.C. carried out mouse necropsies. A.A., M.S.F.-G., M.T.F.-G. and G.H. performed histopathological analysis. J.d.l.R., M.F., Y.L and H.P. did bioinformatics analysis. J.d.l.R, C.L.-O- and J.C. interpreted results. M.F., S.B.d.Q., I.N., E.M., A.S. and R.F. contributed to some of the experiments. R.R., C.L.-O., A.B. and J.C supervised the study. J.d.l.R. and J.C. wrote the manuscript. All authors discussed the results and commented on the manuscript.

Competing Financial Interests

The authors declare no competing financial interests.

Data Availability Statement- Accession codes: RNA-seq data from mouse tumors for the identification of fusion transcripts and from transcriptomic profiling of BPH-1 and RWPE-1 cell lines supporting the findings of this study have been deposited in ArrayExpress with the accession codes E-ERAD-610 (https://www.ebi.ac.uk/arrayexpress/experiments/E-ERAD-610/) and E-ERAD-432, (https://www.ebi.ac.uk/arrayexpress/experiments/E-ERAD-432/), respectively.

Code availability. Python scripts used for the fusion transcript analysis are available upon request.

Europe PMC Funders Author Manuscripts

[9]Centro de Investigación Biomédica en Red de Cáncer, Spain

Abstract

The overwhelming amount of genetic alterations identified through cancer genome sequencing requires complementary approaches to interpret their significance and interactions. We developed a novel whole-body insertional mutagenesis screen in mice, designed for the discovery of *Pten*-cooperating tumor suppressors, in which mobilization of a single-copy inactivating *Sleeping Beauty* transposon is coupled to *Pten* disruption within the same genome. The analysis of 278 transposition-induced prostate, breast and skin tumors detected tissue-specific and shared datasets of known and candidate cancer genes. We validated *ZBTB20*, *CELF2*, *PARD3*, *AKAP13* and *WAC,* identified by our screens in multiple cancer types, as new tumor suppressors in prostate cancer: we demonstrated their synergy with *PTEN* for preventing invasion *in vitro* and confirmed their clinical relevance. Further characterization of *Wac in vivo* revealed obligate haploinsufficiency for this autophagy-regulating gene in a *Pten*-deficient context. Our study identifies complex *PTEN*-cooperating tumor suppressor networks in different cancer types with potential clinical implications.

Introduction

Although cancer genome sequencing has revealed multiple genetic modifications underlying the carcinogenic process1, its ability to pinpoint players altered by non-genetic mechanisms is limited and discerning between driver and passenger alterations still represents a major challenge. Moreover, such strategy is not designed to elucidate cooperation between multiple driver genes. Indeed, some genes previously thought to be passengers are now believed to cooperate with other cancer genes and thus become drivers2.

Insertional mutagenesis in mice is a valuable method for genome-wide functional studies. Transposon-based somatic screens have identified new genes involved in the pathogenesis of different cancer types. Transposon mobilization in mice with known cancer-predisposing mutations has also uncovered synergistic mechanisms between networks driving cancer progression3–13. Here, we have enhanced the capabilities of transposon-based insertional mutagenesis to identify cooperating cancer driver events, developing a system that allows disruption of a known targeted gene and single-copy transposon mobilization to occur simultaneously in the same cell. Using this strategy, we performed a mutagenesis screen in mice aimed at identifying loss-of-function alterations cooperating with the inactivation of *Pten*, a tumor suppressor commonly deleted/mutated in cancer. In parallel, for comparison with a more conventional setting, we generated another cohort of mice harbouring an additional concatemer of inactivating transposons.

A single transposon was sufficient to cause cancer in cooperation with *Pten* loss. The analysis of prostate, breast and skin tumors from these mice allowed the identification of large numbers of *Pten*-cooperating tumor suppressor candidate genes. Focusing on the prostate, we confirmed the functional and clinical relevance of 5 of these candidates (*ZBTB20*, *CELF2*, *PARD3*, *AKAP13* and *WAC*) for cancer progression. Finally, *in vivo*

Europe PMC Funders Author Manuscripts

validation in a prostate-specific *Pten*-deficient background revealed that the autophagy-regulating gene *Wac* is a novel obligate haploinsufficient tumor suppressor.

Results

A *Sleeping Beauty*-dependent inactivatable *Pten* allele

To uncover tumor suppressors collaborating with Pten-deficiency in cancer progression, we generated mice carrying a *Pten* allele inactivatable upon *Sleeping Beauty* (SB)-mediated transposition ($Pten^{SBm2/+}$) (Fig. 1a and Supplementary Fig. 1a-f). Briefly, *Pten* exon 5, containing the phosphatase domain, was flanked by two SB terminal repeats (TRs). In the absence of SB, the *Pten* allele functions normally, but it becomes inactivated upon SB transposase-mediated mobilization of the transposon, which can be reinserted in the genome, potentially generating an additional loss-of-function mutation in another locus of the same cell. As demonstrated by an *Hprt* trapping assay, the mobilized *Pten* exon 5, bearing its natural splice acceptor, functions as a gene disrupting element (Supplementary Fig. 2a).

$Pten^{SBm2/+}$ mice were intercrossed with mice carrying the *SB11* transposase into the *Rosa26* locus ($Rosa26^{SB11/SB11}$), to induce transposition, and a mutant *Bloom* allele ($Blm^{m3/m3}$), to favor loss of heterozygosity (LOH) of the inactivating genetic events, as Bloom (Blm) deficiency increases mitotic recombination14,15. This produced $Pten^{SBm2/+}$; $Rosa26^{SB11/+}$; $Blm^{m3/m3}$ mice (hereafter PSB, n=59). Additionally, to enrich the number of transposon-induced mutations in each cell, a concatemer with ~35 copies of an inactivating transposon (ITP2m) was established in a subset of mice: $Pten^{SBm2/+}$; ITP2m; $Rosa26^{SB11/+}$; $Blm^{m3/m3}$ (hereafter PISB, n=86) (Fig. 1b and Supplementary Fig. 2b). Also, ITP2m; $Rosa26^{SB11/+}$; $Blm^{m3/m3}$ (hereafter ISB, n=15) and $Rosa26^{SB11/+}$; $Blm^{m3/m3}$ (hereafter SB, n=15) mice were generated as controls. Mice were monitored and sacrificed at the onset of signs of morbidity.

Identification of *Pten*-cooperating tumor suppressors

PSB and PISB mice presented a wide range of neoplastic lesions including prostate, breast, skin, endometrial, intestinal and adrenal tumors with high incidence, as well as lymphomas, thyroid, lung and ureter tumors (Fig. 1c,d and data not shown). These corresponded to cancer types commonly observed in *Pten*-deficient mouse models16. Mean survival was shorter in the PISB cohort compared to the PSB cohort (337 versus 419 days; $P < 0.0001$; log-rank test) (Fig. 1e) although both groups showed similar incidence of total and malignant tumors (Fig. 1c). These results reveal synergy between $Pten^{SBm2}$ and ITP2m in accelerating tumorigenesis.

To identify transposon integrations we performed Illumina sequencing of sheared and barcoded tumor DNA as previously described17. We sequenced 127 prostate tumors (PSB: 45; PISB: 82), 26 breast tumors (PSB: 12; PISB: 14) and 125 skin tumors (PSB: 43; PISB: 82) yielding 1,193,651 non-redundant transposon insertions with a minimal read coverage of 2. Subsequently, we applied statistical analyses based on Gaussian Kernel Convolution separately to six datasets, corresponding to the insertions identified in tumors from the same tissue (prostate, breast or skin) and in the same mouse cohort (PSB or PISB), to identify

genomic loci hit significantly more frequently than predicted by chance18. These common insertion sites (CIS) are likely to contain cancer driver genes. As SB shows tendency to re-integrate close to the transposon donor locus (a phenomenon known as local hopping)14,19, we excluded CIS mapping to the donor chromosomes (19 for *Pten*^{SBm2} and 14 for ITP2m), producing lists of 190 and 1170 CIS respectively from the PSB and PISB prostate tumors, 101 and 291 CIS from the PSB and PISB breast tumors, and 287 and 665 CIS from the PSB and PISB skin tumors (Table 1 and Supplementary Tables 1-7).

717 CIS were exclusively found in the prostate, 191 were breast-specific and 329 were only detected in the skin tumors, whereas 101 were common to all 3 tumor types. Of these, 7 were present in the 6 CIS lists generated from both PSB and PISB mice in prostate, breast and skin tumors, including well-known *Pten*-cooperating genes (*Nf1*, *Cul3* and *Tnrc6b*) and candidate tumor suppressors (*Kansl1*, *Arih1*, *Dyrk1a* and *Chd2*) (Fig. 1f and Supplementary Table 8) 12,20–22. In summary, these genome-wide screens reveal comprehensive sets of tumor suppressor genes that cooperate with *Pten* in a global or tissue-specific manner.

Coupled *Pten*-inactivation and transposition mimic human prostate tumorigenesis

We focused on prostate cancer considering its high incidence in humans and in our mice, as well as the central role of PTEN in its pathogenesis. *Pten*$^{+/-}$ mice develop non-invasive prostate tumors with incomplete penetrance23, whereas complete tumor penetrance is observed upon prostate-specific *Pten*-inactivation24. The presence of concomitant genetic alterations in *Pten*$^{+/-}$ mice has also been shown to trigger prostate cancer progression25–30. The combination of the *Pten*^{SBm2} allele and the SB transposase in PSB and PISB mice should facilitate the coupled inactivation of *Pten* and cooperating tumor suppressors. Moreover, Blm deficiency should favor LOH of both the inactivated *Pten* allele and the transposon-targeted loci, accelerating tumor formation and progression.

In agreement with these predictions, all PSB (n=38) and PISB (n=49) males showed prostate gland enlargement, which, in a high proportion (50% and 72%, respectively), progressed to invasive adenocarcinoma (Fig. 1c). As in human prostate cancer, progression was accompanied by decrease of Pten protein levels and correlative increase in the proportion of actively proliferating, Ki67 positive, cells. Moreover, the contiguity of p63 staining observed in normal epithelium and in prostate intraepithelial neoplasias (PIN) was lost in invasive adenocarcinomas (Fig. 2a,b). In addition, *Pten* LOH was detected in 9/9 analyzed tumors (Fig. 2c). These data indicate that prostate tumorigenesis in our model mirrors the progression of human prostate cancer, confirming its suitability for the molecular characterization of this malignancy.

Prostate CISs are enriched in human cancer genes

Interestingly, 70% of the genes found in PSB overlap with those in PISB ($P < 2.2 \times 10^{-16}$; Fisher's exact test) (Fig. 2d and Supplementary Table 7), indicating that the same signaling pathways support prostate cancer development in both cohorts (significant overlaps were also observed in breast, $P = 3.6 \times 10^{-16}$, and skin tumors, $P < 2.2 \times 10^{-16}$; Fisher's exact test; Supplementary Fig. 3a,d and Supplementary Table 7). To explore the biological and clinical relevance of the genes identified in the prostate tumors, we determined their enrichment in

genes known to be involved in human cancer. CIS genes with human homologues (hCISs) in PSB (hCISs=160) and PISB tumors (hCISs=1047), as well as those shared between both groups (referred to as PSB∩PISB hCISs=115) were analyzed independently. PSB, PISB and PSB∩PISB hCISs were significantly enriched in known and candidate cancer genes listed respectively in the Cancer Gene Census database (CGC) (PSB, $P = 5.50 \times 10^{-16}$; PISB, $P < 2.2 \times 10^{-16}$; PSB∩PISB, $P = 1.22 \times 10^{-14}$, Fisher's exact test) and the Network of Cancer Genes (NCG)31 (PSB, $P = 0.005377$; PISB, $P = 4.27 \times 10^{-7}$; PSB∩PISB, $P = 0.003752$; Fisher's exact test) (Supplementary Fig. 4a,b and Supplementary Tables 9-10). This highlights the potential of combining human cancer sequencing with transposon-based screening for prioritizing and cross-validating candidate cancer genes.

We next asked whether hCIS were enriched in human prostate cancer genes. Genomic rearrangements and copy number variations represent a major source of DNA alteration in prostate cancers. Given the exclusive inactivating capacity of our transposons, we compared the list of hCISs to genes recurrently deleted in human prostate cancer. The analysis of 336 primary prostate tumors from The Cancer Genome Atlas (TCGA) revealed that a significant proportion of PSB, PISB and PSB∩PISB hCISs genes were homozygously deleted in this sample set ($P = 0.01945$, $P = 1.82 \times 10^{-6}$, $P = 0.01042$, respectively; Fisher's exact test) (Supplementary Fig. 4c and Supplementary Table 11). Moreover, considering only TCGA deleted genes which were also downregulated in prostate cancer led to sharply increased significance of the intersections ($P = 0.00088$, $P = 4.74 \times 10^{-10}$, $P = 0.00086$, respectively; Fisher's exact test), further supporting the involvement of these genes as tumor suppressors (Supplementary Fig. 4d,e and Supplementary Table 12).

General features of PSB and PISB prostate cancer CIS genes

To identify genes contributing to prostate cancer progression, we focused on the curated PSB∩PISB hCISs (117 mouse genes corresponding to 115 human orthologues) (Supplementary Table 13). The analysis of their transposon integration pattern (as well as of those of breast and skin tumors) revealed the presence of insertions scattered along these genes, consistent with tumor suppressor functions (Supplementary Figs. 5-7). Accordingly, RNAseq analysis of PSB and PISB prostate tumors identified chimeric transcripts of CIS genes where transposon insertions caused disruption of their reading frames (Supplementary Table 14).

To demonstrate the significance of these CIS genes, we studied their distribution among the tumors analyzed. As shown in figure 2e, a number of genes are hit in most neoplasms (a phenomenon also seen in breast and skin tumors; Supplementary. Fig. 3b,e), with a median of 20 and 33 hits per prostate tumor in the PSB and PISB cohorts, respectively. The presence of multiple hits per tumor in the single-transposon cohort supports the co-existence of multiple tumor subclones with different insertions cooperating with *Pten*-disruption within a tumor. This is in line with recent human studies providing evidence for polyclonality in prostate cancer32–34. Genes frequently mutated in the PSB tumors were also highly mutated in the PISB cohort ($R = 0.82$, $P < 2.2 \times 10^{-16}$) (Fig. 2f), demonstrating their importance for driving prostate cancer. Significant positive correlations are also detectable in

breast ($R = 0.77$, $P = 1.17 \times 10^{-4}$) and skin ($R = 0.88$, $P < 2.2 \times 10^{-16}$) tumors (Supplementary Fig. 3c,f).

To explore the potential cooperation of these genes with PTEN-inactivation in driving prostate tumorigenesis, we evaluated the mRNA expression levels of *PTEN* and our list of PSB∩PISB genes in human prostate tumors from the TCGA, Taylor35 and Barbieri36 datasets. Of note, the PSB∩PISB hCIS set is highly enriched in genes whose mRNA expression levels correlate with those of *PTEN*, which might reflect a tendency for PSB∩PISB hCIS genes to be co-regulated with *PTEN* (Fig. 2g). This finding suggests the validity of our screen for pinpointing genes involved in *PTEN*-related processes in prostate cancer.

Deregulated pathways in PSB and PISB prostate cancers

To deepen into the molecular and biological function of the prostate PSB∩PISB CIS genes, we applied DAVID gene-set enrichment analysis37 using KEGG, BioCarta and GO-term datasets (Fig. 3a and Supplementary Table 15) (for similar breast and skin CIS analyses see Supplementary Tables 16 and 17). Chromatin/histone modifying enzymes constitute one of the most significantly enriched pathways. Histone methylase genes such as *ARID1A* or those of members of the MLL protein family (*MLL1*, *MLL5*) are recurrently mutated in prostate cancer, in association with advanced disease stages36,38. Moreover, they interact with the androgen receptor (AR), a key player in prostate tumorigenesis38. Additionally, loss of the histone acetylase CREBBP cooperates with *PTEN* haploinsufficiency in driving prostate cancer39.

We identified a large number of genes involved in RNA stability, splicing and transcriptional regulation. The homeodomain transcription factors *MEIS1* and *PBX1*, known oncogenes for other malignancies, are down-regulated at various stages of prostate cancer progression40. Our results constitute the first *in vivo* indication of their tumor suppressive role in the prostate. In the case of *Pbx1*, transposon distribution and chimeric transcript data support this view (Supplementary Fig. 5 and Supplementary Table 14). Similarly, the gene encoding transcription factor FOXP1 has been described as an oncogene or a tumor suppressor, depending on the context4,41. The distribution of insertions along *Foxp1* in our screen points to a tumor suppressor role, in agreement with recent findings in human prostate cancer42 (Supplementary Fig. 5). Another interesting transcription factor hit by our screen and known to be altered in prostate cancer is *ETV6*. Unlike other ETS genes, *ETV6* is not involved in gene fusions in human prostate tumors. Instead, *ETV6* is hemizygously deleted in ~25% of clinically localized prostate cancer, consistent with our results43.

Genes involved in ubiquitin-mediated proteolysis were also significantly enriched, especially E3-ubiquitin ligases. Exome sequencing of 112 prostate adenocarcinomas has previously revealed the substrate-binding subunit of CUL3-based E3 ligase, named *SPOP*, as the gene most frequently mutated in this malignancy36. The *Cul3* CIS in our screen suggests that alterations in other members of this E3-ligase complex may have similar consequences.

Alterations in intracellular membrane trafficking, intercellular communication or cytoskeleton organization also emerged as important molecular networks which can

compromise cell polarity. PTEN plays essential roles in cellular polarization, in part by recruitment to the endocytic vesicles44,45. Thus, the PTEN-interacting polarity protein PARD3, a tumor suppressor in different tumor types but unexplored in prostate cancer, comes up as an interesting candidate.

Finally, our screens identified alterations of central signaling networks in prostate cancer such as androgen receptor (AR) signaling (*Nrip1*, *Yy1*, *Mll1*, *Mll5*, *Foxp1*), RAS/MAPK (*Rasa1*, *Nf1*, *Erbb2ip*) and PI3K/AKT (*Pik3r1*, *Magi3, Pten* ceRNAs). In fact, a large number of putative *Pten* competitive endogenous RNAs (ceRNAs), including the validated ceRNAs *Cnot6l* and *Tnrc*6b20,46 were present among our CISs. In the polyclonal PSB and PISB tumors, disruption of *Pten* ceRNAs would further decrease Pten function in those subclones without *Pten* LOH. In a previous SB screen focusing on melanoma, 33 *Pten* ceRNAs were identified20. We found a significant overlap between these and our CIS genes (PSB, $P = 6.58 \times 10^{-10}$; PISB, $P < 2.2 \times 10^{-16}$; PSB∩PISB, $P = 3.63 \times 10^{-11}$; Fisher's exact test) (Supplementary Fig. 8a and Supplementary Table 18). Moreover, our CIS genes were significantly enriched among the *PTEN* ceRNAs predicted by the ceFINDER algorithm47 (PSB, $P = 4.51 \times 10^{-12}$; PISB, $P < 2.2 \times 10^{-16}$, PSB∩PISB, $P = 2.44 \times 10^{-10}$; Fisher's exact test) (Supplementary Fig. 8b and Supplementary Table 19).

Co-silencing of *PTEN* and candidate genes drives invasion

To explore the role of the identified genes in the evolution of cancer, we used small interfering RNAs (siRNAs) to silence the expression of candidate genes in two immortalized but non-transformed human prostate cell lines, named BPH-1 and RWPE-1. In contrast to cancer cells, immortalized cells resemble more closely the primary cells they derive from and, therefore, do not contain cancer driving genetic alterations. Thus, we tested the effect of inhibiting the expression of our CIS genes, either alone or in combination with *PTEN*-silencing, on their invasive ability *in vitro*.

We selected five of the twenty genes most frequently hit by transposons in our screens, which were not annotated in the Cancer Gene Census and for which a role in prostate cancer had not been described so far (Fig. 3b and Table 1). These genes are *ZBTB20* (Zinc finger and BTB domain containing 20), *CELF2* (CUGBP, Elav-Like Family member 2), *AKAP13* (A-Kinase Anchor Protein 13), *PARD3* (Par-3 family cell polarity regulator) and *WAC* (WW domain containing Adaptor with Coiled-coil). Co-silencing of *PTEN* together with each of the candidates in BPH-1 and RWPE-1 cells sharply increased their invasiveness (Fig. 4a, Supplementary Fig. 9 and Supplementary Table 20). This synergistic effect is consistent with a cooperative role of these genes with *PTEN* in preventing malignant progression.

Oncogenic pathways disrupted by co-silencing

To examine the molecular basis of this phenotype, we performed RNAseq transcriptomic profiling of BPH-1 and RWPE-1 cell lines upon candidate silencing or co-silencing with *PTEN* (Supplementary Fig. 10 and Supplementary Tables 21-25). Principal component analysis revealed that the first component was determined by the cell line, whereas the second component discriminated single-gene knock-down from co-silencing conditions (Fig

4b). This suggests rewiring of common molecular pathways irrespective of the gene being co-silenced with *PTEN*.

Pathway enrichment analysis of transcriptional changes associated with co-silencing (versus single *PTEN*-silencing), showed common themes shared by the candidates (Fig. 4c and Supplementary Tables 26-35). Among the upregulated genes, enrichment was detected for pathways promoting cancer progression: epithelial-mesenchymal transition, MYC-dependent transcriptional activation, MET/RAS/MAPK signaling and PI3K/AKT/MTOR signaling. Accordingly, Western blot analysis showed that, compared with single *PTEN*-silencing, co-silencing of each of the candidates induced increased levels of p-AKT and/or p-mTOR without further reduction of PTEN levels (Supplementary Fig. 11). The downregulated genes were enriched in pathways including mitotic spindle formation, Rho GTPases, DNA damage response, TGFβ and androgen receptor (AR) signaling. *PTEN* deletion in human and murine prostate tumors has been previously described to decrease the AR transcriptional output, as the PI3K and AR oncogenic pathways cross-regulate each other by reciprocal feedback48. Several of these pathways (AR, RAS/MAPK and PI3K/AKT) are also overrepresented in the PSB∩PISB CIS from prostate tumors.

Clinical relevance of validated genes

We then analyzed the mRNA expression of these genes in prostate tumors from the TCGA dataset. *ZBTB20*, *CELF2*, *PARD3*, *AKAP13* and *WAC* mRNA levels were significantly reduced in primary prostate cancer samples (n=336) compared with benign tissues (n=65) (Fig. 5a). To investigate more advanced stages of the disease, we analyzed the Taylor dataset35, including primary (n=131) and metastatic samples (n=29). We observed a further reduction of mRNA expression of these genes upon progression to metastasis (Fig. 5b). Additionally, a positive correlation was detected in primary tumors between *PTEN* and *ZBTB20*, *CELF2*, *PARD3* and *WAC* gene expression (Fig. 5c). This is stronger (and extensive to *AKAP13*) when more advanced tumors are included in the analysis (Fig 5d), supporting the cooperation between *PTEN* and these genes in preventing cancer progression. With the exception of *CELF2*, correlation is clearer for *PTEN* log2 expression levels above 8.5. Although gene-expression independent regulatory mechanisms might operate, this could also reflect that the contribution of *ZBTB20*, *PARD3*, *AKAP13* and *WAC* to prevent cancer progression is stronger when PTEN function is perturbed, but not lost. In addition to these observations, recurrence-free survival of patients with tumors expressing low levels of these genes was strikingly reduced (Fig. 5e). This was also true for *ZBTB20*, *AKAP13* and *WAC* when the analysis was restricted to primary tumors (Supplementary Fig. 12). Altogether, these results highlight the clinical relevance of the *PTEN*-cooperating tumor suppressor genes identified.

Wac: a new obligate haploinsufficient prostate cancer gene

To explore the *in vivo* effects of *Wac* disruption on mouse prostate tumorigenesis, we generated a mouse model with prostate-specific *Pten* homozygous inactivation combined with prostate-specific *Wac* heterozygous/homozygous deletion. Tumor development in these mice disclosed complex interactions between *Wac* and *Pten* deficiencies. Compared with prostate-specific $Pten^{\Delta/\Delta}$ mice, prostate-specific $Pten^{\Delta/\Delta}$; $Wac^{+/\Delta}$ mice developed larger

tumors, whereas prostate-specific *Pten*$^{\Delta/\Delta}$; *Wac*$^{\Delta/\Delta}$ mice were protected from tumor progression (Fig. 6a). This reveals a phenomenon of obligate haploinsufficiency by which, under *Pten*-deficiency, partial *Wac* inactivation potentiates tumor growth, whereas complete *Wac* inactivation precludes it.

The tumor promoting effect of partial *Wac* inactivation is more evident at earlier cancer development stages: it leads to significantly increased tumor sizes in 4-month old *Pten*$^{\Delta/\Delta}$; *Wac*$^{+/\Delta}$ mice, whereas only a tendency towards larger tumors is observed 5 months later (Fig. 6a,b). This is consistent with the proposed role of *Wac* as an activator of autophagy, a process known to exert dual effects on cancer, suppressing tumor initiation and promoting the growth of established cancers[49–52].

Discussion

PTEN, the second most frequently mutated/deleted gene in human cancer, is a key controller of signaling nodes in multiple tumor types[53,54]. Based on a novel strategy which couples targeted gene inactivation to single-copy transposon mobilization, we have performed a genome-wide survey for genes cooperating with *Pten* in suppressing tumorigenesis in mice. Our model recapitulates the progressive histological, immunohistochemical and genetic alterations of human prostate cancer, confirming its suitability for the molecular characterization of this malignancy. Our studies revealed comprehensive landscapes of tissue-specific and global *Pten*-collaborating genes, pathways and biological processes, including RNA metabolism, chromatin remodeling or ubiquitin-mediated proteolysis. Previous work has proven the utility of transposon-based somatic mutagenesis to identify and validate candidate cancer genes[4–8,10–13]. Our strategy meets these objectives and opens novel applications of somatic transposition by introducing relevant features.

First, the single-copy transposon limits the number of insertions to one per cell, which is aimed at reducing the number of passenger insertions and increasing the specificity of the screen. To our knowledge, this is the first time a single-copy transposon has been shown to generate significant CISs in a somatic mutagenesis screen. Second, our approach achieves transposon-dependent targeted gene disruption, favoring the identification of insertions cooperating with the engineered mutation (in our case, *Pten*-inactivation). Transposons have been successfully used before together with Cre-dependent activation/inactivation of known oncogenes/tumor suppressors, including *Pten*[3,6,8,11–13]. However, using a Cre-inactivated *Pten*-floxed allele does not guarantee perfect coupling of *Pten*-inactivation and transposon mobilization. In contrast, in our model transposition only happens in cells that have undergone *Pten*-inactivation, avoiding the development of transposon-induced tumors with intact *Pten*. Third, our screen exclusively involves inactivating transposition. Although this precludes the identification of potential oncogenes, it facilitates interpretation of the roles of uncharacterized candidate genes.

Detailed analysis of prostate cancer CISs showed enrichment in known (CGC) and putative (NCG) cancer genes. All genes had insertions evenly distributed along their loci, the pattern expected for tumor suppressors. Consistently, they overlap significantly with genes combining homozygous deletions and downregulation of their expression in TCGA human

prostate cancer samples. In addition, they are enriched in genes whose expression levels positively correlate with those of *PTEN* in human prostate cancer, supporting the specificity of the screen to pinpoint *PTEN*-cooperating genes. We prioritized our characterization/validation efforts on 5 genes ranking among the 20 most frequently hit prostate cancer CIS and not previously described as cancer drivers. We confirmed the effect of *ZBTB20*, *CELF2*, *PARD3*, *AKAP13* and *WAC* genetic inhibition in *Pten*-deficient contexts to enhance invasion and unleash canonical cancer-promoting pathways, and we provided evidence of their clinical relevance in human prostate cancer. Finally, we characterized *Wac* as a new obligate haploinssuficient tumor suppressor *in vivo*.

Wac obligate haploinsufficiency agrees with its proposed role as an autophagy activator 50,51. Co-silencing of *WAC* and *PTEN* resulted in the downregulation of pathways directly related to autophagy, such as KEGG_LYSOSOME and KEGG_PEROXISOME (FDR q-values = 0.000) (Supplementary Table 35). Heterozygous disruption of *Becn1*, a Wac-interacting gene essential for autophagy, increases the frequency of spontaneous malignancies and accelerates HBV-induced hepatocellular carcinogenesis55. However, liver tumors arising from *becn1* allelic loss do not undergo LOH, suggesting obligate haploinsufficiency49. In addition, autophagy abrogation by complete loss of *Atg7* delays *Pten*-deficient prostate tumor progression56. Our results parallel these observations, as heterozygous *Wac* deletion promotes prostate tumor progression, whereas its complete loss constrains it. Autophagy exerts dual effects on cancer, suppressing initiation but promoting growth of established cancers49,52. Accordingly, *Wac* inactivation leads to significantly larger tumors in 4-month old $Pten^{\Delta/\Delta}$; $Wac^{+/\Delta}$ mice, but only a tendency is observed 5 months later (Fig. 6a,b). These findings, likely to underlie the modest decrease of *WAC* mRNA levels accompanying human prostate cancer progression, are relevant for basic and translational oncology. Moreover, the dependence of *Pten*-deficient tumors on Wac function opens potential opportunities for drug development.

Our approach recapitulates the sporadic nature of human tumorigenesis, where mutations in relevant cancer genes occur randomly in individual cells from any tissue surrounded by healthy cells. Beyond prostate cancer, mice in our cohorts developed several tumor types for which *Pten* relevance is well documented. Exploration of the potential of the novel putative tumor suppressors to prevent such cancers is warranted. Hopefully, our results will lay the basis for therapeutic strategies inspired in the tumor suppressor networks identified through this screen.

Online Methods

Mouse strains

All animal experiments were conducted in accordance with the guidelines of the Animal Scientific Procedures Act 1986 and the Committee on Animal Experimentation of the University of Oviedo. $Rosa26^{SB11}$ transposase knock-in, *Bloom* mutant (Blm^{m3}), prostate-specific *PB-Cre4* deleter and *Flpo* deleter mice were previously described14,15. $Wac^{tm2a(EUCOMM)Wtsi}$ mice were obtained from the Wellcome Trust Sanger Institute (International Knockout Mouse Consortium). The generation of $Pten^{SBm2}$ and ITP2m+ mice is described in the following sections. To generate the experimental and control mice used in

the transposon screens, *Pten*^{SBm2}, ITP2m and *Blm*^{m3} mice were successively interbred to generate *Pten*$^{SBm2/+}$; ITP2m; *Blm*$^{m3/m3}$ triple-transgenic mice. At the same time, *Rosa26*^{SB11} mice were crossed with *Blm*$^{m3/m3}$ animals and intercrossed to produce *Rosa26*$^{SB11/SB11}$; *Blm*$^{m3/m3}$ mice. Finally, *Pten*$^{SBm2/+}$; ITP2m; *Blm*$^{m3/m3}$ mice were crossed to *Rosa26*$^{SB11/SB11}$; *Blm*$^{m3/m3}$ mice to obtain *Pten*$^{SBm2/+}$; *Rosa26*$^{SB11/+}$; *Blm*$^{m3/m3}$ (PSB), *Pten*$^{SBm2/+}$; ITP2m; *Rosa26*$^{SB11/+}$; *Blm*$^{m3/m3}$ (PISB), ITP2m +; *Rosa26*$^{SB11/+}$; *Blm*$^{m3/m3}$ (ISB) and *Rosa26*$^{SB11/+}$; *Blm*$^{m3/m3}$ (SB) animals. To generate mice with a Wac conditional knockout allele (referred to as *Wac*$^{tm2c(EUCOMM)Wtsi}$), *Wac*$^{tm2a(EUCOMM)Wtsi}$ knockout-first mice were initially crossed to *Flpo* recombinase transgenic mice to remove the FRT-flanked disrupting cassette57. Subsequently, the offspring carrying the *tm2c* allele was outcrossed to wild type C57BL/6 mice and those animals with the *tm2c* allele and negative for *Flpo* were selected and interbred. To generate prostate-specific deletion of *Pten* and *Wac*, *Pten*^{SBm2}, *Wac*$^{tm2c(EUCOMM)Wtsi}$ and *PB-Cre4* recombinase mice were successively intercrossed to generate the desired genotypes. Only males with the *PB-Cre4* allele were used in breedings with *Pten*^{SBm2} and *Wac*$^{tm2c(EUCOMM)Wtsi}$ mice as Cre expression was reported to occur in the oocytes of *PB-Cre4* females. Control and experimental mice were on a mixed C57BL/6, 129Sv and FVB genetic backgrounds. Mice were assigned to experimental groups based on their genotypes, so no randomization was required. Mice were genotyped by conventional PCR of ear/tail clips using the primers listed in Supplementary Table 36.

Generation of the *Pten*^{SBm2} allele

In the *Pten*^{SBm2} allele, *Pten* exon 5 is flanked by two copies of the natural 5' (left) *Sleeping Beauty* (SB) terminal repeat (TR) (one in direct orientation, and the other one as reverse complement), as this configuration displays enhanced transposition efficiency compared with the native SB transposon58. Each TR is separated from the *Pten* exon 5 by approximately 500 bp of intronic sequences (last 500 bp from intron 4 and first 500 bp from intron 5). To generate the targeting construct, first, an SB TR was introduced into a mouse BAC (343F11) through recombineering. For that, a fragment from pQL2 (a vector originally developed by Qi Liang to place a SB TR into genomic DNA by recombineering, and conferring kanamycin resistance) spanning from the SB TR to the end of the Neo/Kan resistance cassette of pQL2 was amplified by PCR, which was also used to add to each end 70 bp of homology with contiguous regions of *Pten* intron 4 as well as a Lox2272 site in one end (between the 70 bp of homology and the SB TR). EL350 recombineering competent bacteria59 containing the 343F11 mouse BAC were electroporated with this PCR product, and recombinant colonies were isolated by dual chrolamphenicol and kanamycin selection. After this, the region containing *Pten* exon 5 and the first introduced SB TR flanked by 6.7 kb and 5.5 kb of mouse genomic DNA at their 5' and 3' ends, respectively, was retrieved into pBS-DTA through recombineering. For that, EL350 carrying the modified 343F11 mouse BAC were electroporated with a fragment of linear DNA amplified from pBS-DTA (conferring ampicillin resistance) using primers which introduced 5' and 3' tails, each with 70 bases of homology to the boundaries of the genomic regions to be retrieved. Transformed bacteria were selected for ampicillin/kanamycin resistance. After this, mini-preps from the positive EL350 cells were retransformed to segregate mixtures of recombinant and non-recombinant plasmids replicating in the same bacterium. Then, PTSA3 and PTSA4, two short (400 bp each) arms of homology to *Pten* intron 5 were PCR amplified using Phusion

Europe PMC Funders Author Manuscripts

polymerase and DNA from the 343F11 BAC as template. During PCR amplification of PTSA3, a Lox2272 site was attached to its 3' end. PTSA3-Lox2272 and PTSA4 were cloned in pZK5-SB-FRT (developed by Qi Liang to introduce another SB repeat into genomic DNA, and conferring kanamycin resistance (for bacteria) and puromycin resistance (for mammalian cells) in a four-way ligation which also contained the puΔTK cassette extracted from pZK5-SB-FRT. The resulting plasmid was linearized and electroporated into the EL350 cells generated from the previous step. Kanamycin/chloramphenicol resistant bacteria were selected and the completeness of the resulting targeting construct, containing also the second SB repeat 500 bp downstream of *Pten* exon 5 and an FRT flanked puΔTK cassette, was checked by digestion with multiple restriction enzymes and capillary Sanger sequencing. Large quantities of pure plasmid were obtained by Maxi-prep (Qiagen). The NotI linearized targeting vector was electroporated in AB1 ES cells and puromycin resistant clones were selected, expanded and microinjected in blastocysts to generate chimaeric mice, from which knock-in progeny containing the $Pten^{SBm1}$ allele were obtained. These mice were subsequently bred to *Rosa26*-FlpE mice to remove the FRT-flanked puΔTK cassette, and thus generate the $Pten^{SBm2}$ allele.

Generation of the ITP2m concatemer

To generate ITP2m transposons, which have both PB and SB terminal repeats (TRs) and can therefore be mobilized with both transposon systems, TRs were cloned into pBlueScript and the following genetic elements were introduced in between them: an adenovirus splice acceptor (AV-SA), five bidirectional SV40 polyadenylation signals (pA) and a splice acceptor from exon 2 of the mouse *Engrailed-2* gene (En2SA). ITP2m transposons were cut out of pBlueScript and prepared for pronuclear injection using standard techniques as described in Rad et al. 20109.

Necropsy and histopathological analysis

Mice were monitored for tumors at least twice a week and sacrificed before tumor masses compromised their well-being or at the onset of other signs of morbidity. For DNA extraction, tumors were snap-frozen in liquid nitrogen. For histological studies, tumors were fixed in 4% formaldehyde, paraffin-embedded, sectioned and stained with haematoxylin and eosin for morphological examination. Necropsies were performed by several investigators who were not actively blinded to the mouse genotype. Samples were excluded if post-necropsy genotyping did not confirm initial genotyping. Tissue samples were examined by four experienced histopathologists (A.A., M.S.F.-G., M.T.F.-G. and G.H.) blinded to mouse genotypes.

Immunohistochemistry

Sections from tissue micro-arrays containing 114 formalin-fixed paraffin-embedded PSB or PISB mouse tumors were cut at 5 μM for immunohistochemical detection of PTEN, p63 and Ki67 on a DAKO Autostainer. After deparaffinization, heat-induced antigen retrieval was performed. Subsequently, primary antibody incubation was carried out using the following antibodies: mouse monoclonal anti-PTEN (M3627, Agilent Technologies, 1:200), mouse monoclonal anti-p63 (IR662, Agilent Technologies, Ready-to-Use) and rabbit monoclonal anti-ki67 (KI681C01, DCS Innovative Diagnostik-Systeme, 1:150), respectively. Sections

were then incubated with the secondary antibodies anti-mouse (for PTEN and p63) and anti-rabbit (for ki67) from Agilent Technologies for 30 minutes at room temperature, and stained with chromagen DAB (3-3´-diaminobenzidine, Dako). Finally, they were counterstained for 10 minutes with Dako Hematoxilin. Ki67 and Pten staining intensities were graded as negative (-), mild (+), moderate (++) and intense (+++) in the PIN, adenocarcinoma and normal tissue components of each tumor.

Splinkerette PCR and Illumina sequencing

These were done as previously described17.

Identification of common integration sites (CISs)

Transposon insertions were mapped to the mouse genome using the SSAHA2 algorithm. Query sequences were filtered to contain splinkerette primer sequences that were located in the transposon ITRs. Redundant sequences from the same tumor and mapping to the same genomic location were ‘collapsed’ to a single integration. To identify those regions in the genome hit by transposons significantly more frequently than expected by chance (so called CISs), non-redundant insertions were analyzed using a Gaussian Kernel Convolution–based framework18 for different kernel window sizes (from 10 kb to 100 kb, in 10 kb steps, plus an extra 200-kb window). CISs predicted across multiple scales and overlapping in their genomic locations were clustered together, and only the ones obtained using the smallest windows were reported. SfiI, a known artifactual CIS frequently found in transposon screens, was filtered out from the definitive CIS lists. Curated lists were obtained after removal of predicted genes.

RNAseq analysis

RNAseq libraries were constructed using the Illumina TruSeq Stranded RNA protocol with oligo dT pulldown and sequenced on Illumina HiSeq2500 by 75-bp paired-end sequencing. For RNAseq transcriptomic profiling of BPH-1 and RWPE-1 cell lines, analysis was performed using TopHat60 version 2.0.13. Read counts were obtained using HTSeq61 version 0.6.1 and differential expression analysis was performed using the DESeq262 software package version 1.14.1. RNAseq analysis of transposon-CIS RNA chimeric transcripts was done as previously described by Temiz et al.63 Sequencing reads were aligned to the mouse reference genome GRCm38 with exon 5 of *Pten* masked at the locus and the transposon sequence containing *Pten* exon 5 added to the reference as a separate sequence. Alignment to this modified reference genome was performed using GSNAP64 version 2015-11-20 and fusions with *Pten* exon 5 were identified employing our own software implementation in the scripting language Python. Python scripts used for the fusion analysis are available upon request.

Pathway enrichment analysis

Pathway enrichment analysis was performed by DAVID37 (using KEGG, BioCarta and GO-term datasets) and the GSEAPreranked module from GSEA v3.0 (using hallmark and canonical pathways datasets65. Results obtained with DAVID were visualized by the Cytoscape Enrichment Map plugin66.

Gene-silencing and invasion assays

For gene-silencing experiments, BPH-1 and RWPE-1 immortalized human prostate cells, obtained from the American Type Culture Collection (ATCC) and previously checked to exclude mycoplasma contamination, were transfected with 10 nM final concentration of siRNA oligonucleotides purchased from Life Technologies (Silencer Select Pre-Designed and Validated siRNAs) using Lipofectamine RNAi Max (Life Technologies) in Opti-MEM I Reduced Serum Medium without serum (Gibco) following the manufacturer's instructions. Two days later, their invasive potential was evaluated using 24-well Matrigel-coated invasion chambers with an 8 mm pore size (BD Biosciences). For BPH-1, 6 x 10^5 cells were allowed to invade for 72 h using 15% fetal bovine serum as a chemoattractant, whereas for RWPE-1 cells, 8 x 10^5 cells were seeded and allowed to invade for 48 h, using bovine pituitary extract (BPE) and human recombinant epidermal growth factor (EGF) as chemoattractants. Cells that reached the lower surface were stained with crystal violet and counted under the microscope.

SDS-PAGE and Western blot

Cultured cells were homogenized in SDS lysis buffer containing 100 mM Tris-HCl pH 7.4, 2% SDS, 50 mM EDTA pH 8, protease inhibitor cocktail (P8340, Sigma) and phosphatase inhibitor cocktails (P5726 and P0044, Sigma). Protein concentration was evaluated with the bicinchoninic acid assay (Pierce BCA Protein Assay Kit). Equal amounts of proteins (10 μg) were loaded onto 4-20% precast polyacrylamide gels (BioRad). After electrophoresis, gels were electrotransferred onto PVDF membranes (BioRad), blocked with 5% nonfat dry milk in TBS-T buffer (20 mM Tris pH 7.4, 150 mM NaCl, and 0.1% Tween 20) for 1 hour at room temperature and incubated overnight at 4 °C with various primary antibodies: rabbit monoclonal anti-PTEN (9188, Cell Signaling, 1:1000), rabbit monoclonal anti-pAKT (4060, Cell Signaling, 1:1000), rabbit monoclonal anti-AKT (4691, Cell Signaling, 1:1000), rabbit monoclonal anti-pmTOR (2971, Cell Signaling, 1:1000), rabbit monoclonal anti-mTOR (2983, Cell Signaling, 1:1000) or mouse monoclonal anti-GAPDH (G8795, Sigma, 1:10,000). Finally, we incubated the blots with goat anti-rabbit or horse anti-mouse horseradish peroxidase-conjugated secondary antibodies (Cell Signaling) diluted 1:3,000 in 2.5% nonfat dry milk in TBS-T, washed them and developed the immunoreactive bands with Clarity Western ECL (BioRad).

Quantitative RT-PCR

For qRT-PCR, cells were collected 72 h after transfection and total RNA was extracted using the RNeasy Plus Mini kit (Qiagen). cDNA was synthesized with Thermoscript RT-PCR (Invitrogen). qPCR was carried out in triplicate for each sample using 20 ng of cDNA per reaction, TaqMan Universal PCR Master Mix (Applied Biosystems), and 1 μL of TaqMan Gene Expression Assay probes (Life Technologies) for *ZBTB20*, *CELF2*, *PARD3*, *AKAP13*, *WAC* and *GAPDH*, the latter used as an internal control for the amount of template cDNA (Supplementary Fig. 13).

Statistics

We used Microsoft Excel, GraphPad Prism or R version 3.2.0 (The R Project for Statistical Computing, see URL section) software for calculations. Specific statistical tests, number of samples and data representation used in each analysis are indicated along the main text or in the figure legends. Data were checked to meet the assumptions of each test. Size of animal cohorts was estimated on the basis of previous transposon-based somatic cancer screens and after preliminary observations of near 100% penetrance of prostate cancer in PSB and PISB males.

Supplementary Material

Refer to Web version on PubMed Central for supplementary material.

Acknowledgements

We thank staff of the Research Support Facility at the Wellcome Trust Sanger Institute; the Laboratory of Molecular Medicine at IMOMA; and the Transgenic Animal Unit, the Molecular Histopathology Unit, the Department of Biochemistry and Molecular Biology and the Biobank of the Principality of Asturias at IUOPA for excellent technical assistance. This work was supported by grants from the Wellcome Trust (grant no. 098051; author A.B.); the Ministerio de Economía y Competitividad-Spain (grant no. SAF2014-52413, author C.L.-O.); the German Research Society (grant no. SFB1243, author R.R.); as well as by funding from Fundación María Cristina Masaveu Peterson; Fundación Centro Médico de Asturias; Fundación Bancaria Caja de Ahorros de Asturias/Liberbank; FEBS; CIBERONC, Plan Feder; Progeria Research Foundation; EDP Foundation; and the German Cancer Consortium; G.S.V. is funded by a Wellcome Trust Senior Fellowship in Clinical Science (WT095663MA). J.d.l.R. is a recipient of a FEBS Long-Term fellowship. J.C. was a recipient of a FEBS Long-term fellowship in the initial phases of this work. J.d.l.R. was a recipient of a fellowship from Fundación María Cristina Masaveu Peterson during part of this work.

References

1. Alexandrov LB, et al. Signatures of mutational processes in human cancer. Nature. 2013; 500:415–21. [PubMed: 23945592]
2. Davoli T, et al. Cumulative haploinsufficiency and triplosensitivity drive aneuploidy patterns and shape the cancer genome. Cell. 2013; 155:948–62. [PubMed: 24183448]
3. Takeda H, et al. Transposon mutagenesis identifies genes and evolutionary forces driving gastrointestinal tract tumor progression. Nat Genet. 2015; 47:142–50. [PubMed: 25559195]
4. Rad R, et al. A conditional piggyBac transposition system for genetic screening in mice identifies oncogenic networks in pancreatic cancer. Nat Genet. 2015; 47:47–56. [PubMed: 25485836]
5. Moriarity BS, Largaespada DA. Sleeping Beauty transposon insertional mutagenesis based mouse models for cancer gene discovery. Curr Opin Genet Dev. 2015; 30:66–72. [PubMed: 26051241]
6. Mann MB, et al. Transposon mutagenesis identifies genetic drivers of Braf(V600E) melanoma. Nature Genetics. 2015; 47:486–U86. [PubMed: 25848750]
7. Jones KB. Transposon mutagenesis disentangles osteosarcoma genetic drivers. Nat Genet. 2015; 47:564–5. [PubMed: 26018893]
8. Vassiliou GS, et al. Mutant nucleophosmin and cooperating pathways drive leukemia initiation and progression in mice. Nat Genet. 2011; 43:470–5. [PubMed: 21441929]
9. Rad R, et al. PiggyBac transposon mutagenesis: a tool for cancer gene discovery in mice. Science. 2010; 330:1104–7. [PubMed: 20947725]
10. Bard-Chapeau EA, et al. Transposon mutagenesis identifies genes driving hepatocellular carcinoma in a chronic hepatitis B mouse model. Nat Genet. 2014; 46:24–32. [PubMed: 24316982]

URLs: The R Project for Statistical Computing, http://www.r-project.org/; Project Betastasis, http://www.betastasis.com.

11. Pérez-Mancera PA, et al. The deubiquitinase USP9X suppresses pancreatic ductal adenocarcinoma. Nature. 2012; 486:266–70. [PubMed: 22699621]
12. Rangel R, et al. Transposon mutagenesis identifies genes that cooperate with mutant Pten in breast cancer progression. Proc Natl Acad Sci U S A. 2016; 113:E7749–E7758. [PubMed: 27849608]
13. Ahmad I, et al. Sleeping Beauty screen reveals Pparg activation in metastatic prostate cancer. Proc Natl Acad Sci U S A. 2016; 113:8290–5. [PubMed: 27357679]
14. Dupuy AJ, Akagi K, Largaespada DA, Copeland NG, Jenkins NA. Mammalian mutagenesis using a highly mobile somatic Sleeping Beauty transposon system. Nature. 2005; 436:221–6. [PubMed: 16015321]
15. Luo G, et al. Cancer predisposition caused by elevated mitotic recombination in Bloom mice. Nat Genet. 2000; 26:424–9. [PubMed: 11101838]
16. Hollander MC, Blumenthal GM, Dennis PA. PTEN loss in the continuum of common cancers, rare syndromes and mouse models. Nat Rev Cancer. 2011; 11:289–301. [PubMed: 21430697]
17. Friedrich MJ, et al. Genome-wide transposon screening and quantitative insertion site sequencing for cancer gene discovery in mice. Nat Protoc. 2017; 12:289–309. [PubMed: 28079877]
18. de Ridder J, Uren A, Kool J, Reinders M, Wessels L. Detecting statistically significant common insertion sites in retroviral insertional mutagenesis screens. PLoS Comput Biol. 2006; 2:e166. [PubMed: 17154714]
19. Collier LS, Carlson CM, Ravimohan S, Dupuy AJ, Largaespada DA. Cancer gene discovery in solid tumours using transposon-based somatic mutagenesis in the mouse. Nature. 2005; 436:272–6. [PubMed: 16015333]
20. Karreth FA, et al. In vivo identification of tumor- suppressive PTEN ceRNAs in an oncogenic BRAF-induced mouse model of melanoma. Cell. 2011; 147:382–95. [PubMed: 22000016]
21. Keng VW, et al. PTEN and NF1 inactivation in Schwann cells produces a severe phenotype in the peripheral nervous system that promotes the development and malignant progression of peripheral nerve sheath tumors. Cancer Res. 2012; 72:3405–13. [PubMed: 22700876]
22. Dorr C, et al. Transposon Mutagenesis Screen Identifies Potential Lung Cancer Drivers and CUL3 as a Tumor Suppressor. Mol Cancer Res. 2015; 13:1238–47. [PubMed: 25995385]
23. Alimonti A, et al. Subtle variations in Pten dose determine cancer susceptibility. Nat Genet. 2010; 42:454–8. [PubMed: 20400965]
24. Trotman LC, et al. Pten dose dictates cancer progression in the prostate. PLoS Biol. 2003; 1:E59. [PubMed: 14691534]
25. Ai J, et al. Concomitant loss of EAF2/U19 and Pten synergistically promotes prostate carcinogenesis in the mouse model. Oncogene. 2014; 33:2286–94. [PubMed: 23708662]
26. Patel R, et al. Sprouty2, PTEN, and PP2A interact to regulate prostate cancer progression. J Clin Invest. 2013; 123:1157–75. [PubMed: 23434594]
27. Fernández-Marcos PJ, et al. Simultaneous inactivation of Par-4 and PTEN in vivo leads to synergistic NF-kappaB activation and invasive prostate carcinoma. Proc Natl Acad Sci U S A. 2009; 106:12962–7. [PubMed: 19470463]
28. Carver BS, et al. Aberrant ERG expression cooperates with loss of PTEN to promote cancer progression in the prostate. Nat Genet. 2009; 41:619–24. [PubMed: 19396168]
29. Abate-Shen C, et al. Nkx3.1; Pten mutant mice develop invasive prostate adenocarcinoma and lymph node metastases. Cancer Res. 2003; 63:3886–90. [PubMed: 12873978]
30. Di Cristofano A, De Acetis M, Koff A, Cordon-Cardo C, Pandolfi PP. Pten and p27KIP1 cooperate in prostate cancer tumor suppression in the mouse. Nat Genet. 2001; 27:222–4. [PubMed: 11175795]
31. An O, et al. NCG 4.0: the network of cancer genes in the era of massive mutational screenings of cancer genomes. Database-the Journal of Biological Databases and Curation. 2014
32. Gundem G, et al. The evolutionary history of lethal metastatic prostate cancer. Nature. 2015; 520:353–7. [PubMed: 25830880]
33. Cooper CS, et al. Analysis of the genetic phylogeny of multifocal prostate cancer identifies multiple independent clonal expansions in neoplastic and morphologically normal prostate tissue. Nat Genet. 2015; 47:367–72. [PubMed: 25730763]

34. Boutros PC, et al. Spatial genomic heterogeneity within localized, multifocal prostate cancer. Nat Genet. 2015; 47:736–45. [PubMed: 26005866]
35. Taylor BS, et al. Integrative genomic profiling of human prostate cancer. Cancer Cell. 2010; 18:11–22. [PubMed: 20579941]
36. Barbieri CE, et al. Exome sequencing identifies recurrent SPOP, FOXA1 and MED12 mutations in prostate cancer. Nat Genet. 2012; 44:685–9. [PubMed: 22610119]
37. Huang da W, Sherman BT, Lempicki RA. Systematic and integrative analysis of large gene lists using DAVID bioinformatics resources. Nat Protoc. 2009; 4:44–57. [PubMed: 19131956]
38. Grasso CS, et al. The mutational landscape of lethal castration-resistant prostate cancer. Nature. 2012; 487:239–43. [PubMed: 22722839]
39. Ding L, et al. CBP loss cooperates with PTEN haploinsufficiency to drive prostate cancer: implications for epigenetic therapy. Cancer Res. 2014; 74:2050–61. [PubMed: 24491799]
40. Chen JL, et al. Deregulation of a Hox protein regulatory network spanning prostate cancer initiation and progression. Clin Cancer Res. 2012; 18:4291–302. [PubMed: 22723371]
41. Koon HB, Ippolito GC, Banham AH, Tucker PW. FOXP1: a potential therapeutic target in cancer. Expert Opin Ther Targets. 2007; 11:955–65. [PubMed: 17614763]
42. Takayama K, et al. Integrative analysis of FOXP1 function reveals a tumor-suppressive effect in prostate cancer. Mol Endocrinol. 2014; 28:2012–24. [PubMed: 25329375]
43. Demichelis F, et al. Distinct genomic aberrations associated with ERG rearranged prostate cancer. Genes Chromosomes Cancer. 2009; 48:366–80. [PubMed: 19156837]
44. Naguib A, et al. PTEN functions by recruitment to cytoplasmic vesicles. Mol Cell. 2015; 58:255–68. [PubMed: 25866245]
45. Leslie NR, Batty IH, Maccario H, Davidson L, Downes CP. Understanding PTEN regulation: PIP2, polarity and protein stability. Oncogene. 2008; 27:5464–76. [PubMed: 18794881]
46. Tay Y, et al. Coding-independent regulation of the tumor suppressor PTEN by competing endogenous mRNAs. Cell. 2011; 147:344–57. [PubMed: 22000013]
47. Sarver AL, Subramanian S. Competing endogenous RNA database. Bioinformation. 2012; 8:731–3. [PubMed: 23055620]
48. Carver BS, et al. Reciprocal feedback regulation of PI3K and androgen receptor signaling in PTEN-deficient prostate cancer. Cancer Cell. 2011; 19:575–86. [PubMed: 21575859]
49. White E. Deconvoluting the context-dependent role for autophagy in cancer. Nat Rev Cancer. 2012; 12:401–10. [PubMed: 22534666]
50. McKnight NC, et al. Genome-wide siRNA screen reveals amino acid starvation-induced autophagy requires SCOC and WAC. EMBO J. 2012; 31:1931–46. [PubMed: 22354037]
51. Joachim J, et al. Activation of ULK Kinase and Autophagy by GABARAP Trafficking from the Centrosome Is Regulated by WAC and GM130. Mol Cell. 2015; 60:899–913. [PubMed: 26687599]
52. Fernández AF, López-Otín C. The functional and pathologic relevance of autophagy proteases. J Clin Invest. 2015; 125:33–41. [PubMed: 25654548]
53. Yin Y, Shen WH. PTEN: a new guardian of the genome. Oncogene. 2008; 27:5443–53. [PubMed: 18794879]
54. Milella M, et al. PTEN: Multiple Functions in Human Malignant Tumors. Front Oncol. 2015; 5:24. [PubMed: 25763354]
55. Qu X, et al. Promotion of tumorigenesis by heterozygous disruption of the beclin 1 autophagy gene. J Clin Invest. 2003; 112:1809–20. [PubMed: 14638851]
56. Santanam U, et al. Atg7 cooperates with Pten loss to drive prostate cancer tumor growth. Genes Dev. 2016; 30:399–407. [PubMed: 26883359]
57. Skarnes WC, et al. A conditional knockout resource for the genome-wide study of mouse gene function. Nature. 2011; 474:337–42. [PubMed: 21677750]
58. Izsvak Z, et al. Involvement of a bifunctional, paired-like DNA-binding domain and a transpositional enhancer in Sleeping Beauty transposition. J Biol Chem. 2002; 277:34581–8. [PubMed: 12082109]

59. Lee EC, et al. A highly efficient Escherichia coli-based chromosome engineering system adapted for recombinogenic targeting and subcloning of BAC DNA. Genomics. 2001; 73:56–65. [PubMed: 11352566]

60. Kim D, et al. TopHat2: accurate alignment of transcriptomes in the presence of insertions, deletions and gene fusions. Genome Biol. 2013; 14:R36. [PubMed: 23618408]

61. Anders S, Pyl PT, Huber W. HTSeq--a Python framework to work with high-throughput sequencing data. Bioinformatics. 2015; 31:166–9. [PubMed: 25260700]

62. Love MI, Huber W, Anders S. Moderated estimation of fold change and dispersion for RNA-seq data with DESeq2. Genome Biol. 2014; 15:550. [PubMed: 25516281]

63. Temiz NA, et al. RNA sequencing of Sleeping Beauty transposon-induced tumors detects transposon-RNA fusions in forward genetic cancer screens. Genome Res. 2016; 26:119–29. [PubMed: 26553456]

64. Wu TD, Nacu S. Fast and SNP-tolerant detection of complex variants and splicing in short reads. Bioinformatics. 2010; 26:873–81. [PubMed: 20147302]

65. Subramanian A, et al. Gene set enrichment analysis: a knowledge-based approach for interpreting genome-wide expression profiles. Proc Natl Acad Sci U S A. 2005; 102:15545–50. [PubMed: 16199517]

66. Merico D, Isserlin R, Stueker O, Emili A, Bader GD. Enrichment map: a network-based method for gene-set enrichment visualization and interpretation. PLoS One. 2010; 5:e13984. [PubMed: 21085593]

Europe PMC Funders Author Manuscripts

Europe PMC Funders Author Manuscripts

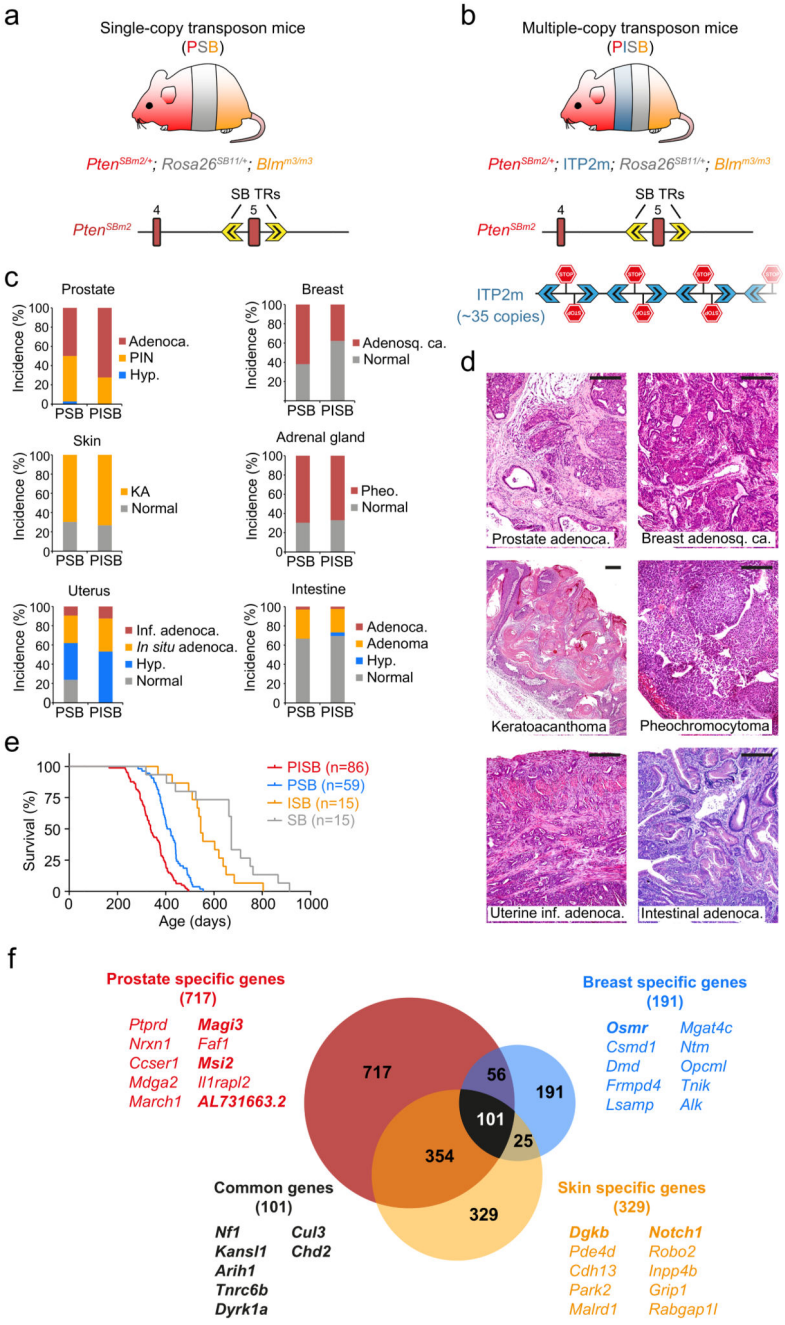

Figure 1. A *Sleeping Beauty*-dependent inactivatable *Pten* allele for coupled whole-body mutagenesis and tumor suppressor discovery in mice.

(a,b) Transposon-bearing mice used in this study. **(a)** Single-copy transposon mice (PSB, *Pten*$^{SBm2/+}$; *Rosa26*$^{SB11/+}$; *Blm*$^{m3/m3}$) harbor the novel *Pten*^{SBm2} allele, in which *Pten* exon 5 is flanked by two *Sleeping Beauty* terminal repeats (SB TRs). This converts the whole cassette into an inactivating transposon which can be mobilized and reintegrated in the genome by the SB transposase, concurrently deleting *Pten* exon 5. **(b)** Multiple-copy transposon mice (PISB, *Pten*$^{SBm2/+}$; ITP2m; *Rosa26*$^{SB11/+}$; *Blm*$^{m3/m3}$), carry *Pten*^{SBm2} and

Europe PMC Funders Author Manuscripts

a new concatemer with ~35 copies of an inactivating transposon (ITP2m) compatible with SB and *PiggyBac* (PB) transposases. **(c)** Tumor incidence in PSB (n=59: n♂=38 + n♀=21) and PISB (n=86: n♂=49 + n♀=37) mice. Adenoca., adenocarcinoma; PIN, prostatic intraepithelial neoplasia; Hyp., hyperplasia; Pheo., pheochromocytoma; KA, keratoacanthoma; Adenosq. ca., adenosquamous carcinoma; inf, infiltrating. **(d)** Photomicrographs of H&E staining in PSB and PISB tumors. Scale bars, 200 μm. **(e)** Kaplan-Meier survival plot of PSB, PISB, ISB and SB mice. PSB versus PISB ($P < 0.0001$), ISB ($P < 0.0001$), SB ($P < 0.0001$); PISB versus ISB ($P < 0.0001$), SB ($P < 0.0001$); ISB versus SB ($P = 0.0253$); log-rank test. **(f)** Venn diagram of prostate, breast and skin CIS genes. The top ten most highly mutated genes specific for each tumor type and seven genes found in all three tumor types in both PSB and PISB cohorts are listed. Genes in bold were found in both PSB and PISB screens.

Europe PMC Funders Author Manuscripts

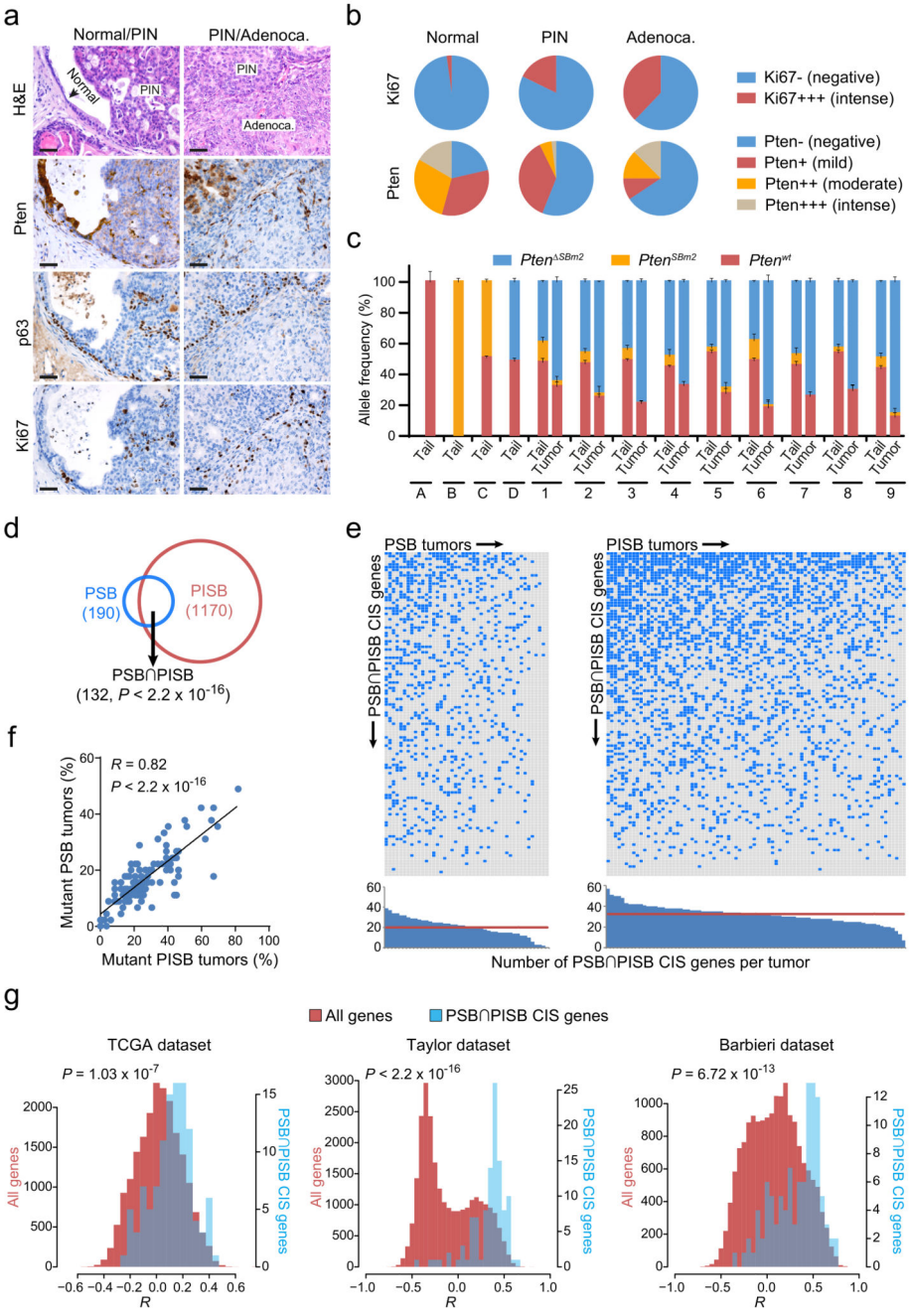

Figure 2. Characterization of *Pten*-inactivated prostate cancer and identification of large sets of genes potentially driving its progression.

(a) H&E, Pten, p63 and Ki67 stainings of normal tissue, PIN and adenocarcinoma lesions from PSB/PISB mice. Scale bars, 50 μm. **(b)** Ki67 and Pten staining quantification in normal tissue, PIN and adenocarcinoma components from 114 PSB/PISB prostate tumors. **(c)** Quantitative PCR for detection/quantification of different *Pten* alleles in tail/tumor pairs from nine PSB/PISB mice (1 to 9). $Pten^{\Delta SBm2}$ represents the targeted *Pten* allele after transposon mobilization. Tails from $Pten^{wt/wt}$ (A), $Pten^{SBm2/SBm2}$ (B), $Pten^{SBm2/wt}$ (C) and

Europe PMC Funders Author Manuscripts

Pten$^{\Delta SBm2/wt}$ (D) mice were used as controls. **(d)** Overlap between PSB (n=190) and PISB (n=1170) prostate CIS genes. $P < 2.2 \times 10^{-16}$; Fisher's exact test. **(e)** Distribution of PSB∩PISB hCIS genes across the 127 prostate tumors analyzed. Blue boxes highlight PSB∩PISB hCIS genes containing SB insertions in each tumor. Histograms show the number of PSB∩PISB hCIS genes with insertions per each tumor. Red horizontal lines represent the median of PSB∩PISB hCIS genes with insertions in PSB/PISB tumors. **(f)** Correlation between the frequency of PSB/PISB prostate tumors with insertions in each PSB∩PISB hCIS gene (n=117). *R*, Pearson correlation coefficient. $P < 2.2 \times 10^{-16}$; Pearson's correlation test. **(g)** Histograms of the Pearson correlation coefficients (*R*) between the mRNA expression of *PTEN* and that of PSB∩PISB hCIS genes (blue bars) or that of all genes in the genome (red bars) in human prostate tumors from TCGA (n=336), Taylor (n=160) and Barbieri (n=31) datasets. *P*-values were calculated by Kolmogorov-Smirnov test.

Europe PMC Funders Author Manuscripts

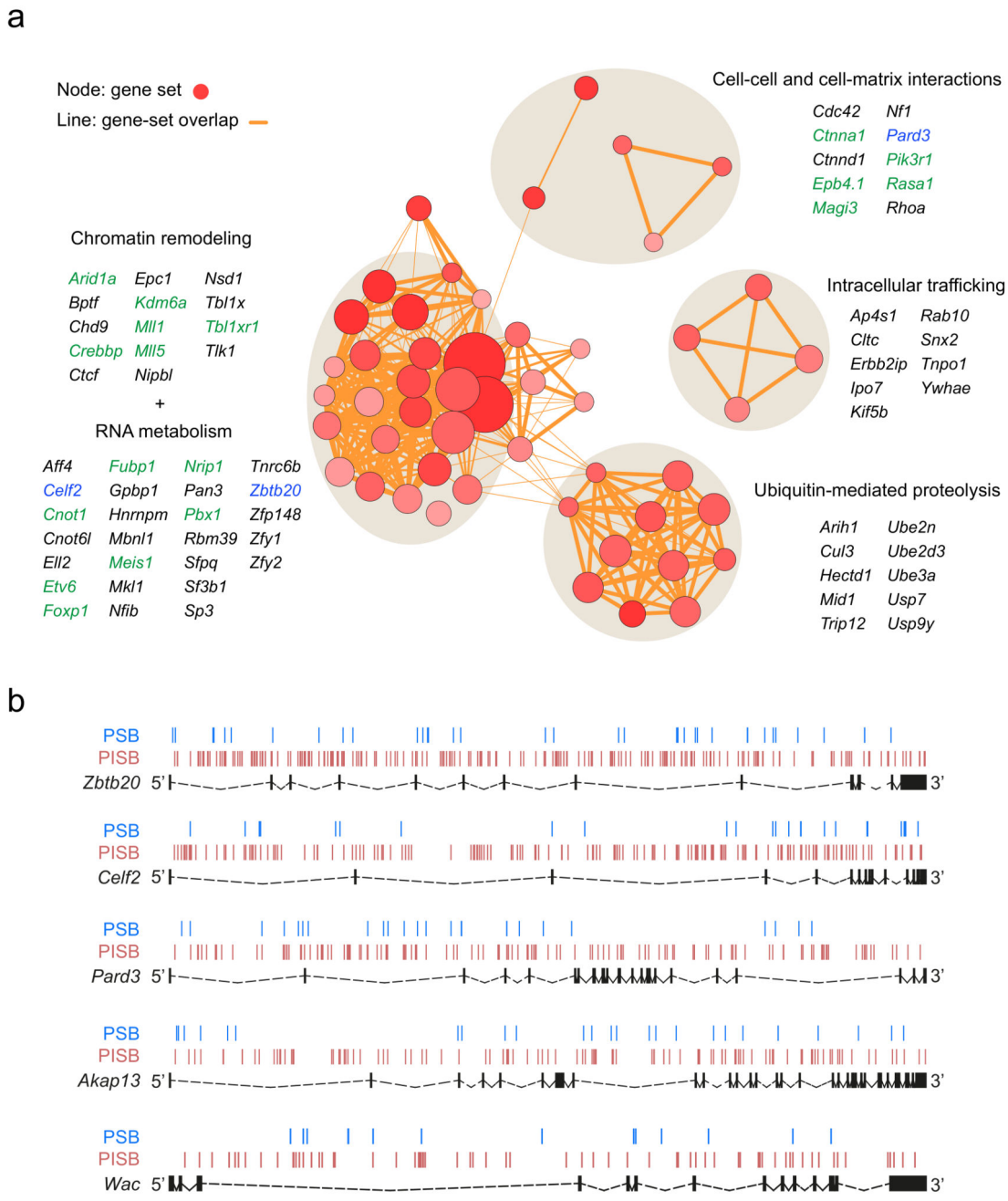

Figure 3. Perturbed biological pathways, cellular processes and novel tumor suppressor candidates enriched among the PSB∩PISB CIS genes.

(a) Enrichment results on the 117 PSB∩PISB CIS genes obtained by DAVID analysis are mapped as a network of gene-sets (nodes) grouped according to their similarity. Only those gene-sets with a Benjamini q-value < 0.1 are represented. Red circles represent nodes (gene-sets). Orange lines represent overlapping between nodes. Node size is proportional to the total number of PSB∩PISB CIS genes in each gene-set. Higher node color intensity represents greater enrichment significance (lower Benjamini q-value) of a particular gene-

set. Line thickness shows the degree of overlap (shared genes) between gene-sets. Groups of functionally related gene-sets are circled (round grey shadows) and labelled, and representative genes for each of them are shown. Genes in green are described to be altered in human prostate cancer. Genes in blue represent three out of the five new tumor suppressor genes identified and validated in this work. **(b)** SB transposon insertion pattern across *Zbtb20*, *Celf2*, *Pard3*, *Akap13* and *Wac* in PSB (blue lines) and PISB (red lines) tumors. Exons are represented as black boxes and introns as dashed lines.

Europe PMC Funders Author Manuscripts

Europe PMC Funders Author Manuscripts

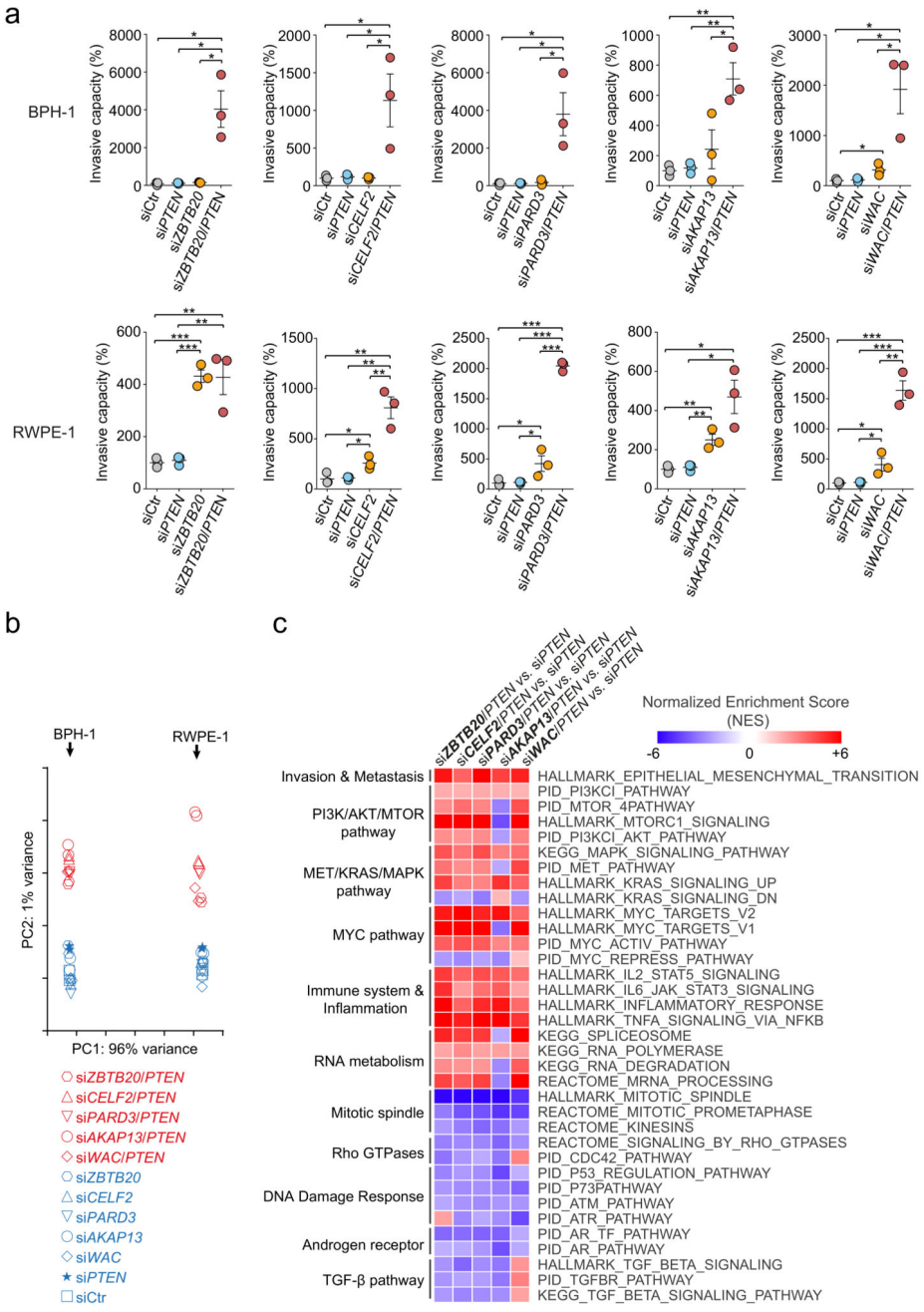

Figure 4. Genetic inhibition of tumor suppressor genes drives prostate cancer progression through canonical signaling pathways.

(a) Effect of *ZBTB20*, *CELF2*, *PARD3*, *AKAP13* and *WAC* silencing, either alone or in combination with *PTEN* interfering, on the invasiveness of BPH-1 (top panel) and RWPE-1 (bottom panel) immortalized human prostate cell lines. Cell invasion rate is expressed as a percentage relative to the mean of control invasion rate values, which was set as 100%. Each circle represents an individual technical replicate. Horizontal lines represent the means and error bars correspond to s.e.m in each condition. *$P < 0.05$, **$P < 0.01$, ***$P < 0.001$, two-

tailed Student's t test. **(b)** Principal component analysis of the RNA-seq expression profiles of RWPE-1 and BPH-1 cell lines upon silencing of the five candidate tumor suppressor genes in **a**, either alone or in combination with *Pten* interfering. RNA expression profiles from siRNA-Ctr- and siRNA-*Pten*-treated cells were also included in the analysis. Component one was determined by the specific cell line being analyzed, whereas component two was determined by the status of single gene silencing versus co-silencing with *Pten*, regardless of the single candidate gene being co-silenced. **(c)** Heatmap depicting a subset of shared deregulated pathways associated to co-silencing of each of the candidate genes, compared with single *Pten*-silencing. Selected pathways shared by at least 4 of the co-silencing conditions and with FDR q-values < 0.025 are represented.

Europe PMC Funders Author Manuscripts

Europe PMC Funders Author Manuscripts

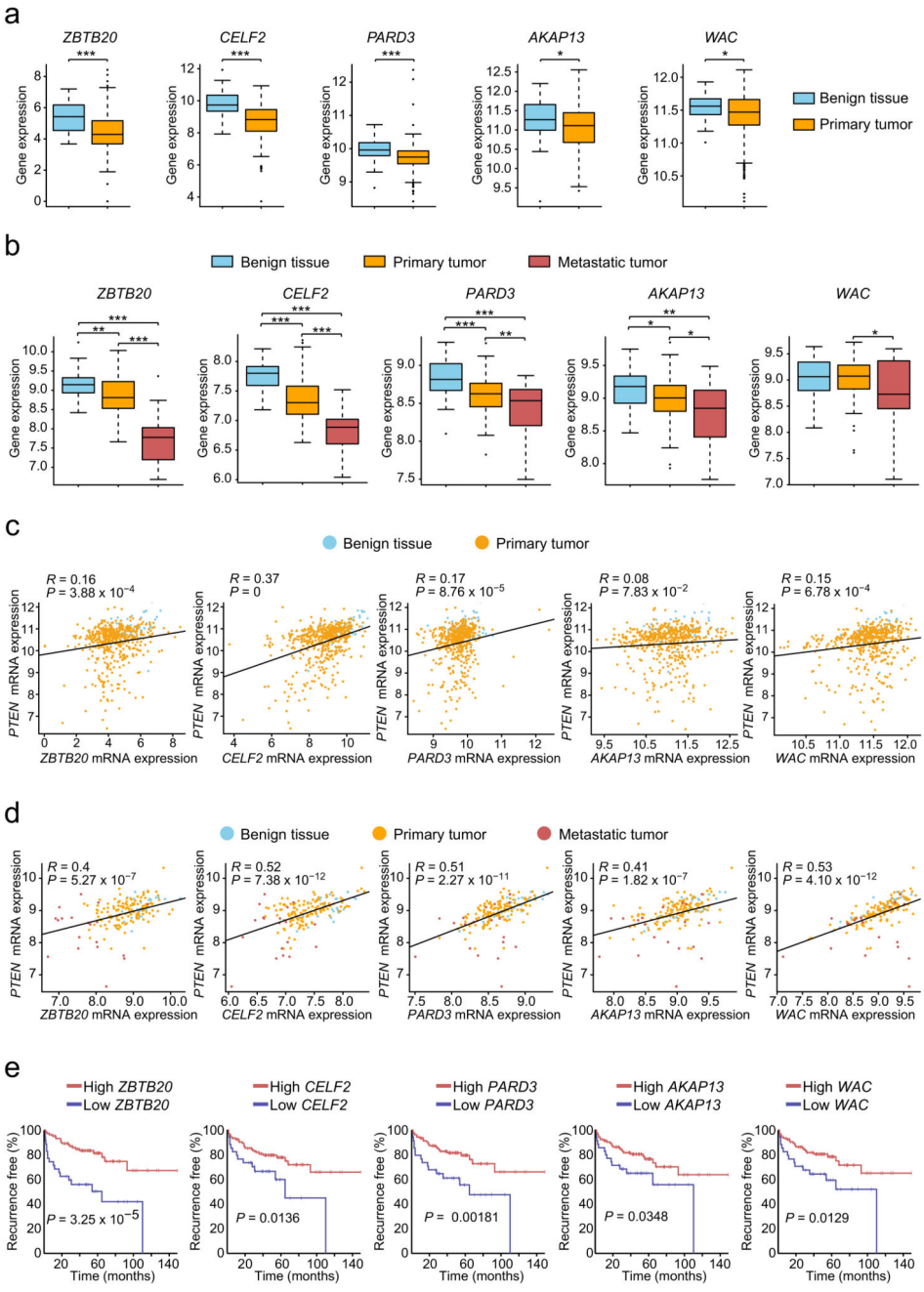

Figure 5. Clinical significance of validated genes in human prostate cancer.

(a) *ZBTB20*, *CELF2*, *PARD3*, *AKAP13* and *WAC* mRNAs are significantly downregulated in primary prostate cancers (n=336) compared to normal tissue samples (n=65) available from TCGA. **(b)** mRNA levels of these genes were further reduced in metastatic samples (n=29) compared to primary tumors (n=131) available from the Taylor dataset. **(a,b)** Boxplots display the 25th to 75th percentiles (boxes), medians (lines), and 1.5 times the interquartile range (whiskers). *$P < 0.05$, **$P < 0.01$, ***$P < 0.001$, two-tailed Student's t test. **(c,d)** Scattered plots show positive correlations between *PTEN* and *ZBTB20*, *CELF2*,

PARD3 and *WAC* gene expression in primary prostate tumors from the TCGA dataset **(c)** and in primary and metastatic tumors from the Taylor **(d)** dataset (in **d**, correlation is also detected for *AKAP13*). *R*, Pearson correlation coefficient. *P*-values were calculated by Pearson's correlation test. Normalized RSEM and log2 mRNA expression values are shown respectively for the TCGA (**a**,**c**) and Taylor (**b**,**d**) datasets. **(e)** Recurrence-free survival Kaplan-Meier analysis of 25% of patients with lowest mRNA expression levels of each of the five genes above versus the remaining 75%. Analyses were performed using the Taylor dataset and the open web interface 'Project Betastasis' (see URLs section). *P*-values were obtained by log-rank test.

Europe PMC Funders Author Manuscripts

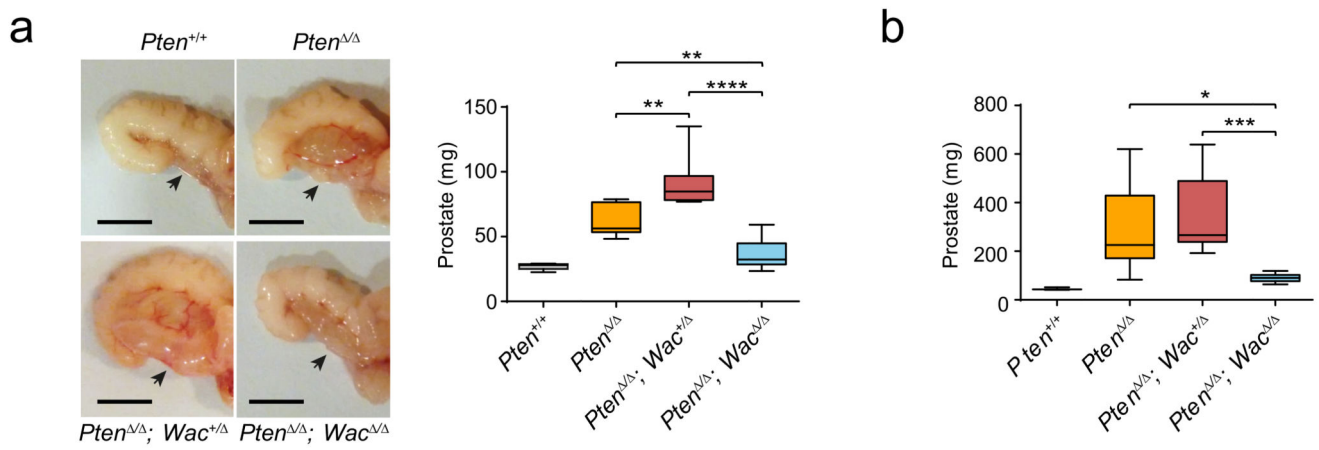

Figure 6. ***In vivo*** **validation of** ***Wac*** **as a new obligate haploinsufficient gene in prostate cancer.**

(a,b) Comparison of anterior prostate lobe tumor weight in 4-month-old mice **(a)** and 9 month-old **(b)** mice of the indicated genotypes. In **a**, n=7 for *Pten*$^{+/+}$, n=7 for *Pten*$^{\Delta/\Delta}$, n=9 for *Pten*$^{\Delta/\Delta}$; Wac$^{+/\Delta}$ and n=8 for *Pten*$^{\Delta/\Delta}$; Wac$^{\Delta/\Delta}$. In **b**, n=3 for *Pten*$^{+/+}$, n=7 for *Pten*$^{\Delta/\Delta}$, n=11 for *Pten*$^{\Delta/\Delta}$; Wac$^{+/\Delta}$ and n=7 for *Pten*$^{\Delta/\Delta}$; Wac$^{\Delta/\Delta}$. Boxplots display the 25th to 75th percentiles (boxes), medians (lines), and the 5th to 95th percentiles (whiskers). *$P < 0.05$, **$P < 0.01$, ***$P < 0.001$, ****$P < 0.0001$, two-tailed Student's t test. Representative pictures of tumors from 4-month-old mice are shown for each genotype **(a)**. Scale bars, 50 mm for all images.

Europe PMC Funders Author Manuscripts

Table 1

Top fifteen PSB∩PISB CIS genes most highly mutated among the 127 prostate, 26 breast and 125 skin tumors analysed.

Genes are ranked according to the percentage of tumors with insertions in each gene. Chr., chromosome.

PSB∩PISB CIS genes	Chr.	% of tumors with insertions			Function or pathway
		Total tumors	PSB tumors	PISB tumors	
Prostate					
Zbtb20	16	70.1	48.9	81.7	Transcription
Lpp	16	58.3	42.2	67.1	Cell adhesion
Celf2	2	57.5	35.6	69.5	Splicing
Pard3	8	55.9	37.8	65.9	Cell polarity
Arid1b	17	53.5	42.2	59.8	Chromatin remodeling
Foxp1	6	51.2	31.1	62.2	Transcription
Nf1	11	49.6	17.8	67.1	RAS signaling
Akap13	7	45.7	37.8	50.0	Small GTPase signaling
Etl4	2	45.7	35.6	51.2	Unknown
Magi3	3	39.4	26.7	46.3	PI3K/PTEN signaling
Nfib	4	38.6	35.6	40.2	Transcription
Tnrc6b	15	38.6	26.7	45.1	PI3K/PTEN signaling
Etv6	6	37.8	24.4	45.1	Transcription
Trip12	1	37.0	24.4	43.9	Ubiquitin mediated proteolysis
Arih1	9	37.0	20.0	46.3	Ubiquitin mediated proteolysis
Breast					
Trps1	15	96.2	91.7	100.0	Transcription
Nf1	11	88.5	75.0	100.0	RAS signaling
Kansl1	11	80.8	75.0	100.0	Chromatin remodeling
Osmr	15	65.4	66.7	64.3	Cytokine receptor
Tnrc6b	15	65.4	50.0	78.6	PI3K/PTEN signaling
Arih1	9	65.4	33.3	92.9	Ubiquitin mediated proteolysis
Cul3	1	57.7	41.7	71.4	Ubiquitin mediated proteolysis
Dyrk1a	16	57.7	41.7	71.4	Protein Kinase
Pias1	9	53.8	25.0	78.6	Protein sumoylation
Ralgapb	2	53.8	50.0	57.1	Small GTPase signaling
Chd2	7	50.0	33.3	64.3	Chromatin remodeling
Uba1	X	42.3	41.7	42.9	Ubiquitin mediated proteolysis
Trp53	11	34.6	25.0	42.9	Tumor suppressor
Hspa4	11	23.1	25.0	21.4	Heat shock protein
Pcsk7	9	11.5	16.7	7.1	Proteolytic enzyme
Skin					
Chl1	6	93.6	86.0	97.6	Cell adhesion

Europe PMC Funders Author Manuscripts

PSB∩PISB CIS genes	Chr.	% of tumors with insertions			Function or pathway
		Total tumors	PSB tumors	PISB tumors	
Celf2	2	76.0	65.1	81.7	RNA metabolism
Dgkb	12	72.8	65.1	76.8	Diacylglycerol kinase
Nfib	4	61.6	62.8	61.0	Transcription
Atxn1	13	61.6	72.1	56.1	Unknown
Tcf12	9	56.8	48.8	61.0	Transcription
Kmt2c	5	55.2	41.9	62.2	Chromatin remodeling
Akap13	7	55.2	51.2	57.3	Small GTPase signaling
Mbnl1	3	54.4	51.2	56.1	Splicing
Arid1b	17	54.4	41.9	61.0	Chromatin remodeling
Nf1	11	52.8	51.2	53.7	RAS signaling
Usp34	11	52.8	46.5	56.1	Ubiquitin mediated proteolysis
Zfand3	17	52.8	44.2	57.3	Unknown
Fchsd2	7	52.0	44.2	56.1	Unknown
Crebbp	16	52.0	44.2	56.1	Chromatin remodeling